Moroccan Journal of Chemistry
ISSN : 2351-812X

Mor. J. Chem., 2023, Volume 11, Issue 3, Page 729-741
https://revues.imist.ma/index.php/morjchem
https://doi.org/10.48317/IMIST.PRSM/morjchem-v11i3.40088

Drug Designing against VP4, VP7 and NSP4 of Rotavirus Proteins – Insilico studies

Mallari Praveen[1*], Alejandro Morales-Bayuelo [1]

[1]*Indira Gandhi National Tribal University Department of Zoology, Amarkantak, Madhya Pradesh, India*
[1]*Grupo GENOMA, Escuela de Medicina, Universidad del Sinú-EBZ, Cartagena, Colombia.*
**corresponding author: Email address: mallaripraveen950@gmail.com*

Received *09 May 2023,*
Revised *15 June 2023,*
Accepted *01 July 2023*

Citation*: Praveen M., Morales-Bayuelo A. (2023) Drug Designing against VP4, VP7 and NSP4 of Rotavirus Proteins – Insilico studies, Mor. J. Chem., 14(6), 729-741.*

Abstract: Rotavirus is predominately infecting infants less than five-year-old children causing acute gastroenteritis, more than two million deaths were reported in 2016. The vaccines constructed were not efficiently preventing the virus infection. However, small molecule discovery from plant-based drugs validation was not done till now against the hetero-oligomeric complex. The methods applied include; VP4, VP7, and NSP4 protein fasta sequences retrieved from the NCBI. The 3D tertiary structures were generated through homology modelling followed validated in Ramachandran plots. The active sites were determined in the Prank Web server. The phytoconstituents (PCs); 396 ligands were retrieved from the IMPPAT database. The proteins and ligands were further docked through Autodock vina after preparing the proteins and ligands in UCSF Chimera and Open Babel. Based on the binding affinity (BA) and No. of hydrogen bond interactions (HBI) further analyzed their DFT studies using Gaussian 09. The docking scores and hydrogen bond interactions of the complexes; Desmal with VP4 complex exhibited -8.7 BA, formed 4 HBI; Salviandulin E with VP7 shown -7.9 BA, formed 5 HBI; Zeylanone with NSP4 has -6.1 BA, formed 4 HBI. Zeylanone have two prior regions in stabilization compared to Desmal and Salviandulin E.

Keywords: *Rotavirus; Spike protein; Enterotoxin; Salviandulin E; Zeylanone*

1. Introduction

Rotavirus (RV) belongs to the 'Reoviridae' family, though there were 9 species (RV A-I), RVA species infect greater than 90% of humans (Kirkwood, 2010). RV is one of the foremost causes for acute gastroenteritis (AGE) among 3- to 5-year-old children (Parashar *et al.,* 2006), which leads to >90% mortality in low-income countries, about greater than two million deaths were reported in the year 2016 (Troeger *et al.,* 2018). Its severity and rapid transmission in temperate regions, predominant in the territories of sub-Saharan Africa and south-east Asia, particularly pronounced in low-income and developing countries (Cook *et al.,* 1990). The victims included not only include humans but also the cattle such as calves, piglets, and poultry (Vlasova *et al.,* 2010).

Virions of RV are non-enveloped with three concentric layers surrounding the surface called Triple Layered Particles (TLP). The genome consists of eleven segmented double standard RNAs, with 6 structural (VP1-4, 6,7) and 6 non-structural (NSP1-6) proteins (Zhang *et al.,* 2018) . The rotavirus antigens (VP4, VP7 and NSP4) stimulate a defensive mechanism in hosts, this complex is referred to

as a hetero-oligomeric complex (Li *et al.,* 2010). These three components together referred to as hetero-oligomeric complexes, have a significant role in the TLP assembly (Maass *et al.,* 1990).

VP4, also known as spike protein is actively involved in increasing its viral progeny via host cell attachment, incorporation, endocytosis modulation, virion morphogenesis and regression (Poruchynsky *et al.,* 1991). VP4 attaches to the host receptor terminal with sialic acid (SA) and thereafter viral proteins interact with various co-receptors such as integrins and hsp70 (Vetter *et al.,* 2022). VP7 is an outer capsid glycoprotein, involved in G-type antigen neutralization and Ca^{2+} dependent while VP4 is a P-type antigen neutralizing antigen (Graham *et al.,* 2003). VP4 and VP7 were responsible for the coating process of the viroplasms. NSP4 sequence translates to 'enterotoxin' as a protein product, actively involved in the perforating of an Endoplasmic Reticulum (ER) membrane by the viroplasms that leads to intestinal secretion and enteric nervous system activation. Enterotoxin is a virulence factor that is secreted out of the gut by the immune system (Matthijnssens *et al.,* 2008). ER membrane is the localizing centre to the VP4, a decrease in Ca^{2+} levels in the endosome releases VP7 and VP4 then disruption of ER regulates (Estes *et al.,* 2003). World Health Organisation (WHO) has certified the 4 live attenuated vaccines. National immunization scheduled two of them Rotarix and Rota Teq, these were effective in controlling the virus's survival (O'Ryan *et al.,* 2009). In recent reports, it was stated that the effect of the vaccine on the virus decreased for the victims (Isanaka *et al.,* 2017).

Previous research studies on curing the illness caused by RVs have focused mostly immune-related vaccines. In this study, we tried to design the natural plant phytoconstituents/bio-actives for small molecule drug discovery validation against the structural proteins (spike protein and outer glycoprotein), non-structural protein (enterotoxin) which were the targets earlier used in designing the vaccine (Diass *et al.,* 2023; Merzouki *et al.,* 2023). In the current study, we utilized the Insilco methodologies in **Figure 1.** such as homology modelling, molecular docking, and density functional theory studies to investigate the potent bioactive molecules which can actively inhibit respective protein activity.

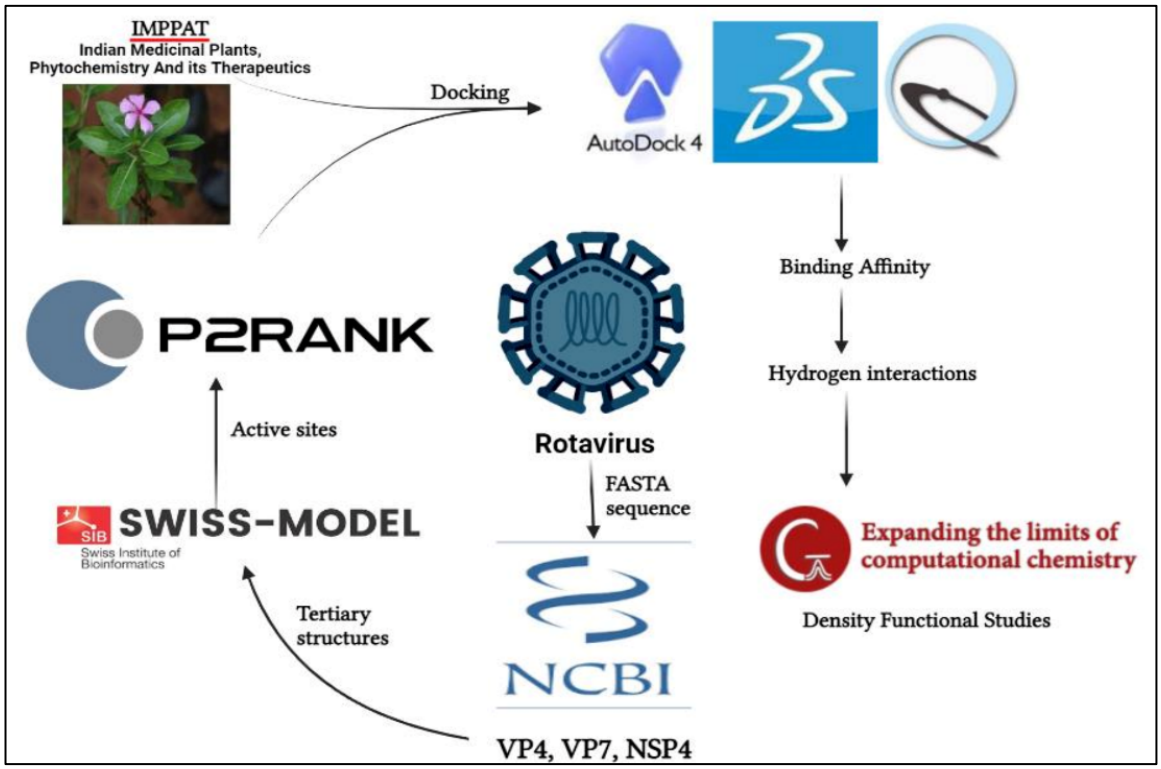

Figure 1. Represents the methodology of the present study

2. Methods and methods

2.1 Sequence retrieval

The Rotavirus's, spike protein (VP4), outer capsid protein (VP7) and enterotoxin (NSP4) sequence retrieved from the National Centre for Biotechnology Information (NCBI) (https://www.ncbi.nlm.nih.gov/) (Medeiros *et al.,* 2023), isolated from the homo sapiens stool samples with the strain G8P bovine DS1 backbone which was deposited recently (i.e., 4th April 2023).

2.2 Homology modelling and validation of 3D structures

The tertiary structures of the proteins were not deposited in the Protein Data Bank (PDB). Thus, the amino acid sequence of each protein is used to generate the tertiary structure of the protein via SWISS-Homology modelling (Bienert *et al.,* 2017). It uses ProMod3 for structural reading of input sequences along with insertions and deletions on an alignment basis, OpenMM and OpenStructure for simulations and comparative modelling followed by parameterisation with the CHARMM22/CMAP force field. The automated models build structures based on the updated sequences from UniProtKB and repository 190,687 PDB structures for template identification, sequence identity and results for QMEAN. The templated-based generated 3D protein structures were validated with the most favored regions (>90%) relying upon the Ramachandran plot which compares how normal or unusual residues geometry compared with the stereochemical quality of the protein structures were used for further analysis.

2.3 Ligand's library preparation

The drugs developed for the disease were plant-based derivatives with modifications in the hit molecules enhanced by the activity of the drug that which played a prominent role in modern drug discovery (Najmi *et al.,* 2022). Indian Medicinal Plants, Phytochemistry and Therapeutics (IMPPAT), IMPPAT database includes the PCs of various indigenous plants with physiochemical properties, drug-likeness rules, and different file formats including the other database IDs deposited such as Pubchem IDs, ZINC and ChEMBL. Three hundred ninety-six (396) ligands retrieved from the IMPPAT database with drug-likeness rules such as Lipinski's Rule of five (RO5) (Lipinski, 2004) with molecular weight less than 500 g/mol (M. wt ≤ 500), hydrogen bond donors not more than five (HBD ≤ 5), hydrogen bond acceptors not more than 10 (HBA≤10), an octanol-water partition coefficient not greater than 5 (logP≤5). Ghose rule (Ghose, 1999) parameters criteria, an octanol-water partition coefficient (log P = -0.4 to 5.6), molecular weight (M. wt = 160 to 480), total number of atoms (NA = 20 to 70) molar refractivity (MR= 40 to 130). The GlaxoSmithKline (GSK) 4/400 rule (Veber, 2002), compounds with an octanol-water partition coefficient (logP>4) and molecular weight (M. wt <400). Pfizer 3/75 rule (Yukawa and Naven, 2020) with low chemical space (ClogP<3) and total polar surface area (TPSA>75). Verber's rule (Vélez *et al.,* 2022) indicates the bioavailability based on rotatable bonds (RB≤10) and polar surface area (PSA≤140). Egan's rule (Egan, 2000) for good bioavailability of two descriptors, total polar surface area (0≥TPSA≤132 Å^2) and octanol-water partition coefficient (-1≥logP≤6). Weighted Quantitative Estimate of drug-likeness (QEDw)[25] with most drug-like scores greater than or equal to 0.7 (QEDw≥0.7).

2.4 Molecular docking

2.4.1 Protein's and Ligand's preparation

The proteins VP4, VP7 and NSP4 generated through homology modelling and validated in the Ramachandran plot were used for docking after preparing each protein without any other residues such as water molecules, het atoms, and ligand groups in the Drug discovery studio (https://3ds.com/products-services/biovia/products) to make a raw protein structure individually. Further, the proteins prepared in Autodock vina on repairing the missing atoms, adding polar hydrogen atoms, checking the torsion angles, and computing the Geister charges. The ligands were downloaded in the sdf format in two-dimensional geometry from the PubChem database (https://pubchem.ncbi.nlm.nih.gov/). Further preparation was carried out by converting the file format to pdbqt through Open Babel (O'Boyle *et al.,* 2011) with three-dimensional optimization in the MMFF6 force field after adding hydrogens.

2.4.2 Grid configuration and Docking

Complete protein structure is not involved in its function, but during the protein folding these active sites are formed and responsible for the binding site to the substrate. The active sites of the built proteins through homology modelling were determined through the PrankWeb server (https://prankweb.cz/) (Radoslav and David, 2018) a ligand binding site of the protein structure prediction server built based on the machine learning method. Based on the probability of the active site scores, the residues were noted. The Grid configurations of the residues were determined through the UCSF Chimera (Pettersen *et al.,* 2004). The binding affinity/free energy between the protein and ligand is calculated through docking. The docking was performed in Autodock Vina (Trott and Olson, 2010) to determine the binding affinity between the complex.

2.5 Density Functional Theory (DFT) based reactivity descriptors.

The present author, in several works, has shown the relationship between quantum similarity and chemical reactivity descriptors (Morales-Bayuelo *et al.,* 2012, Morales-Bayuelo *et al.,* 2017, Morales-Bayuelo and Vivas-Reys, 2012). In addition, the quantum similarity and DFT use the density function as an object of study, the similarity indexes specifically the Coulomb index can be related to electronic factors associated with chemical reactivity. Using the Frontier Molecular Orbitals (FMO) and the energy gap the global reactivity indices, such as chemical potential (μ) (Morales-Bayuelo *et al.,* 2013), hardness (η) (Morales-Bayuelo and Vivas-Reys, 2014) and electrophilicity (ω) (Morales-Bayuelo and Vivas-Reys, 2014), will be calculated. These chemical reactivity indices give an idea about the stability of the systems. The chemical potential (μ) characterizes the tendency of the electrons to escape from the equilibrium system (Morales-Bayuelo and Vivas-Reys, 2014), whereas the chemical hardness (η) is a measure of the resistance of a chemical species to change its electronic configuration (Parr and Pearson, 1983):

$$\mu \approx \frac{E_{LUMO}+E_{HOMO}}{2} \quad \textbf{(3)}$$

And

$$\eta \approx E_{LUMO} - E_{HOMO} \quad \textbf{(4)}$$

The softness is computed by (1/ η). The electrophilicity index (ω) can be interpreted as a measure of the stabilization energy of the system when it is saturated by electrons from the external environment and is mathematically defined as (Geerlings *et al.,* 2013, Chattaraj *et al.,* 2006, Parr *et al.,* 1999, Galván *et al.,* 2000).

$$\omega = \frac{\mu^2}{2\eta} \quad \textbf{(5)}$$

In this work, the local reactivity descriptor is the Fukui functions (equations 6 and 7, f). The equations (6) and (7) represent the response of the chemical potential of a system to changes in the external potential. It is defined as the derivative of the electronic density concerning the number of electrons at the constant external potential:

$$\mathbf{f_k^+ \approx \int_k [\rho_{N+1}(\vec{r}) - \rho_N(\vec{r})] = [q_k(N+1) - q_k(N)]} \quad \textbf{(6)}$$

$$\mathbf{f_k^- \approx \int_k [\rho_N(\vec{r}) - \rho_{N-1}(\vec{r})] = [q_k(N) - q_k(N-1)]} \quad \textbf{(7)}$$

Where (f_k^+) is for nucleophilic attack and (f_k^-) for electrophilic attack (Fuentealba *et al.,* 2022, Pérez and Contreras, 2013). All the structures were developed using M02X/6–31G(d, p) methods in Gaussian 09 package (Frisch *et al.,* 2009)**.**

3. Results and Discussions

3.1 Sequence retrieval

The FASTA format of the Spike protein (VP4), outer capsid protein (VP7) and enterotoxin (NSP4) amino acid sequence was retrieved. Their GenBank accession numbers are as follows; OP374084.1 for VP4, OP311907.1 for VP7, and ON885866.1 for NSP4. Spike protein comprised of 134 residues, outer capsid protein with 284 residues and enterotoxin with 159 residues.

3.2 Homology modelling and the validation of 3D structures

Template-based homology modelling was employed to generate the 3D structures of each protein. VP4 exhibited 74.07% of sequence identity with the depository PDB structure i.e., SPA of trypsin with untreated rotavirus TLP spike protein (PDB ID: 8BP8). VP7 exhibited 85.21% of similarity with VP5/VP8 assemblage of rhesus rotavirus (PDB ID: 6WXE) and NSP4 protein with oligomerised NSP4 domain of rotavirus strain from MF66 of 92.16 percent of sequence similarity (PDB ID: 5Y2H) in **Table 1**. The generated tertiary protein models were further validated in the Ramachandran plot. The green-colored regions depict the most favoured regions or Ramachandran's favored regions mentioned in the graphs. The protein structure amino acids in the most favored regions value calculated in percentage (greater than 90%) are the proper structure and can proceed for further studies. VP4 contains 94.70% of amino acids, VP7 contains 94.12% of amino acids and NSP4 with 98.89% of amino acids in the most favored regions in the Ramachandran plot in **Figure 2**. The three structures contained amino acids in the favored regions on obeying the criteria. Thus, they further investigated molecular docking.

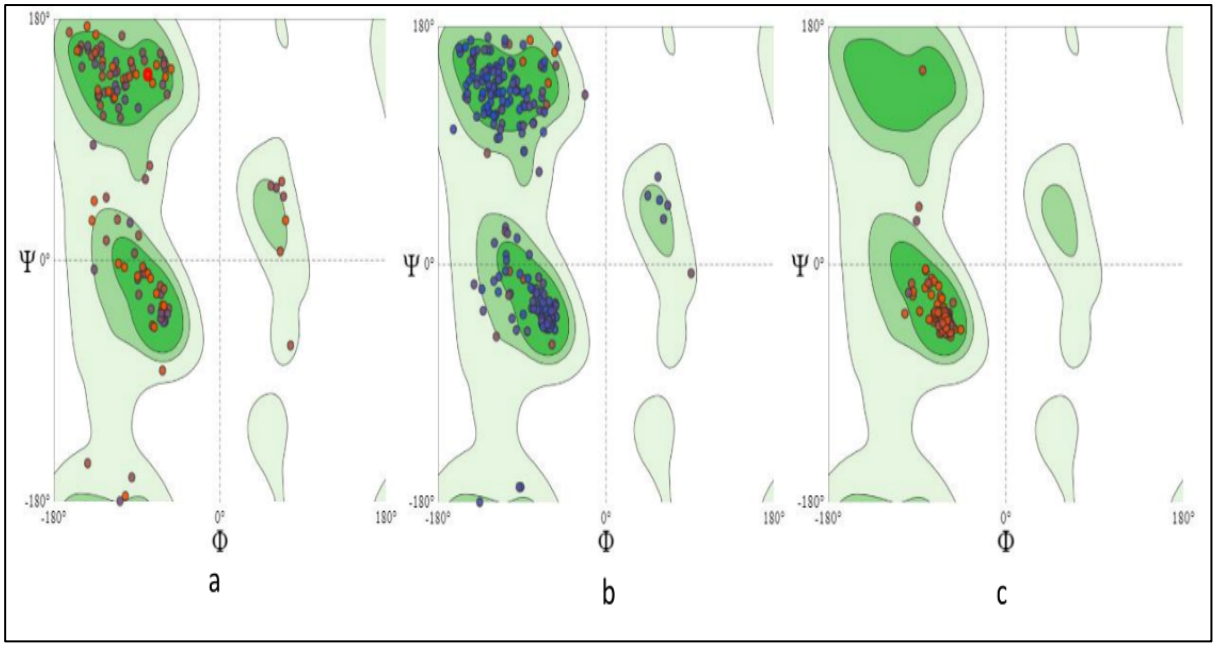

Figure 2. Generated Homology models validation in Ramachandran plots a) VP4 b) VP7 c) NSP4.

Table 1. Template used to generate the 3D models, percentage of sequence identity and validation results in Ramchandran Plot favoured regions determined in SWISS-Homology modelling

Proteins	PDB template	Comments	Seq Identity %	Ramachandran favored (%)
VP4	8BP8	SPA of trypsin untreated rotavirus TLP spike	74.07	94.70
VP7	6WXE	Cryo-EM reconstruction of VP5/VP8 assembly from rhesus rotavirus	85.21	94.12
NSP4	5Y2H	Crystal structure of the oligomerization domain of NSP4 from the rotavirus strain MF66	92.16	98.89

Seq- Sequence, PDB -Protein Data Bank

3.3 Active site prediction

The active sites of each protein was determined from the Prank Web server. The active site probability of VP4 protein was 0.83 with 22 amino acid residues, all of which residue reliably on the C chain peptide. The active site probability of VP7 protein was 0.61 with 10 amino acid residues of V chain peptide. NSP4 active site predicted probability was 0.64 with 11 amino acid residues of B and D chain peptides in **Table 2**.

Table 2. The active sites of the proteins generated from Homology modelling determined in the Prank Web server.

Proteins	Sequences	Chains	Probability of active site	No. of residues at active site
VP4	C_22, C_23, C_24, C_25, C_26, C_28, C_62, C_63, C_64, C_65, C_66, C_68, C_70, C_71, C_73, C_74, C_77, C_82, C_83, C_87, C_88, C_89	C	0.83	22
VP7	V_137, V_138, V_140, V_144, V_145, V_146, V_147, V_149, V_153, V_219	V	0.61	10

NSP4	B_102, B_95, B_98, B_99, D_102, D_105, D_106, D_109, D_113, D_98, D_99	B, D	0.64	11

3.4 Molecular docking

The proteins built through homology modelling and PCs retrieved from IMPPAT were docked to their active sites for determining the binding affinity between them. Each time 396 PCs were docked against each protein and noted their binding affinity values (Supplementary file). In total, the ligands that exhibited the highest binding scores were selected to analyse the number of hydrogen bond interactions. The proteins VP4, VP7 and NSP4 with PCs of in the IMPPAT showed binding scores between -8.8 to -8.5, -8.2 to -7.9, and -6.3 to -6.1 kcal/mol. Further, these complexes were analysed based on the number of hydrogen bonding interactions in **Table 3**.

The interactions of the complexes, in **Figure 3.** VP4 protein with desmal exhibited a binding affinity of -8.7 kcal/mol forms four hydrogen bonds of which three were conventional hydrogen bonds (CHB) and one pi-donor hydrogen bond. The amine groups (NH_2) of C Asn 90 and C Val 91 by donating hydrogen to the ligand's oxygen atom form two CHBs. Another CHB formed between the ligand's donating hydrogen atom with C Pro 93 oxygen atom. A pi-donor hydrogen interaction was observed between the amine group of C Phe 63 with the ligand's pi-orbital.

The binding affinity of VP7 protein with the Salviandulin E was -7.9 kcal/mol, forming five hydrogen bonds. Four CHBs and one Carbon hydrogen bond interaction were formed in the complex. Two CHBs are among the amine groups of V Thr 93 and V Gln 103 that donate the hydrogen to the oxygen atom of the ligand. One of the CHB formed between V Thr 97 OG1 which donated the hydrogen to the ligand's oxygen. Ligand's hydroxyl group by donating a hydrogen atom to the oxygen atom in the V Ser 91 residue makes the fourth CHB. The carbon atom of the ligand that donates the hydrogen to the OE1 V Gln 103 hydrogen acceptor forms a carbon hydrogen bond.

Table 3. The binding affinities of the PCs present in IMPPAT with proteins VP4, VP7 and NSP4; their hydrogen bond interacting residues

IMPPAT ID	B.A. (kcal/mol)	PCs name	PubChem ID	No. of H bonds	Residues
VP4					
IMPHY004801	-8.8	6-Methoxypulcherrimin	44260092	2	C Ile 65, C Asn 90
*IMPHY000655	-8.7	desmal	10018499	4	C Asn 90, C Val 91, C Pro 93, C Phe 63
IMPHY003137	-8.7	Paulownin	3084131	2	C Asn 90, C Phe 63
IMPHY013009	-8.5	Saropyrone	10401833	2	C Cys 74, C Val 23
IMPHY001064	-8.5	alamarine	442157	3	C Asn 87, C Pro 93, C Asn 90
VP7					
IMPHY001506	-8.2	Tinosponone	152154879	4	V Asn 90, V Val 91, V Pro 93, V Phe 63
IMPHY015070	-8.0	sibiricine	179410	1	V Ser 91

IMPHY010431	-8.0	Sibiricine	15070257	1	V Ser 91
IMPHY011520	-7.9	diosbulbin d	21723241	4	^{2}V Ser 91, V Thr 105, V Leu 89
*IMPHY000256	-7.9	Salviandulin E	102251629	5	V Thr 93, V Thr 97, ^{2}V Gln 103, V Ser 91
NSP4					
IMPHY014037	-6.3	hydroxytuberosone	4302704	1	D Thr 101
IMPHY003529	-6.2	3,3'-Bisjuglone	329584	2	^{2}D Thr 101
IMPHY010647	-6.2	Gummadiol	21722930	2	D Thr 102, D Lys 99
*IMPHY004515	-6.1	Zeylanone	5276618	4	D Lys 99, ^{2}D Thr 102, B Asp 98
IMPHY010343	-6.1	Yohimbic Acid	72131	1	D Thr 101

*PCs made a greater number of interactions with the respective proteins

The NSP4 protein with the Zeylanone has a binding affinity of -6.1 kcal/mol and forms four CHBs. One of the CHBs formed by the amine group of D Lys 99 donates hydrogen to the oxygen atom of the ligand. Two CHBs were formed by the sp hybridized OG1 hydrogen donor D Thr 102 with the ligand's oxygen atom, a hydrogen acceptor. The hydrogen atom of the ligand's hydroxyl group is then converted to hydrogen by the residue B Asp 98 OD1 which accepts the hydrogen from it and creates one CHB.

Aoyagi Y et al. reported the antitrypanosomal activity of the Salviandulin E PC from the Salvia leucantha, which was used as a lead compound, synthesized their analogues against Trypanosoma brucei Salviandulin E (Aoyagi *et al.,* 2014). Zeylanone analogues isolated from the Diospyros anisandra plant stem bark reported antiviral activity against influenza virus types A and B, especially during early and middle replication stages in in-vitro studies targeting the nuclear localization protein (Cetina-Montejo *et al.,* 2019). Desmal medicinal/antiviral properties have not been reported previously. This will provide a strong base to pave the way for work on antagonists of the rotavirus spike protein (VP4).

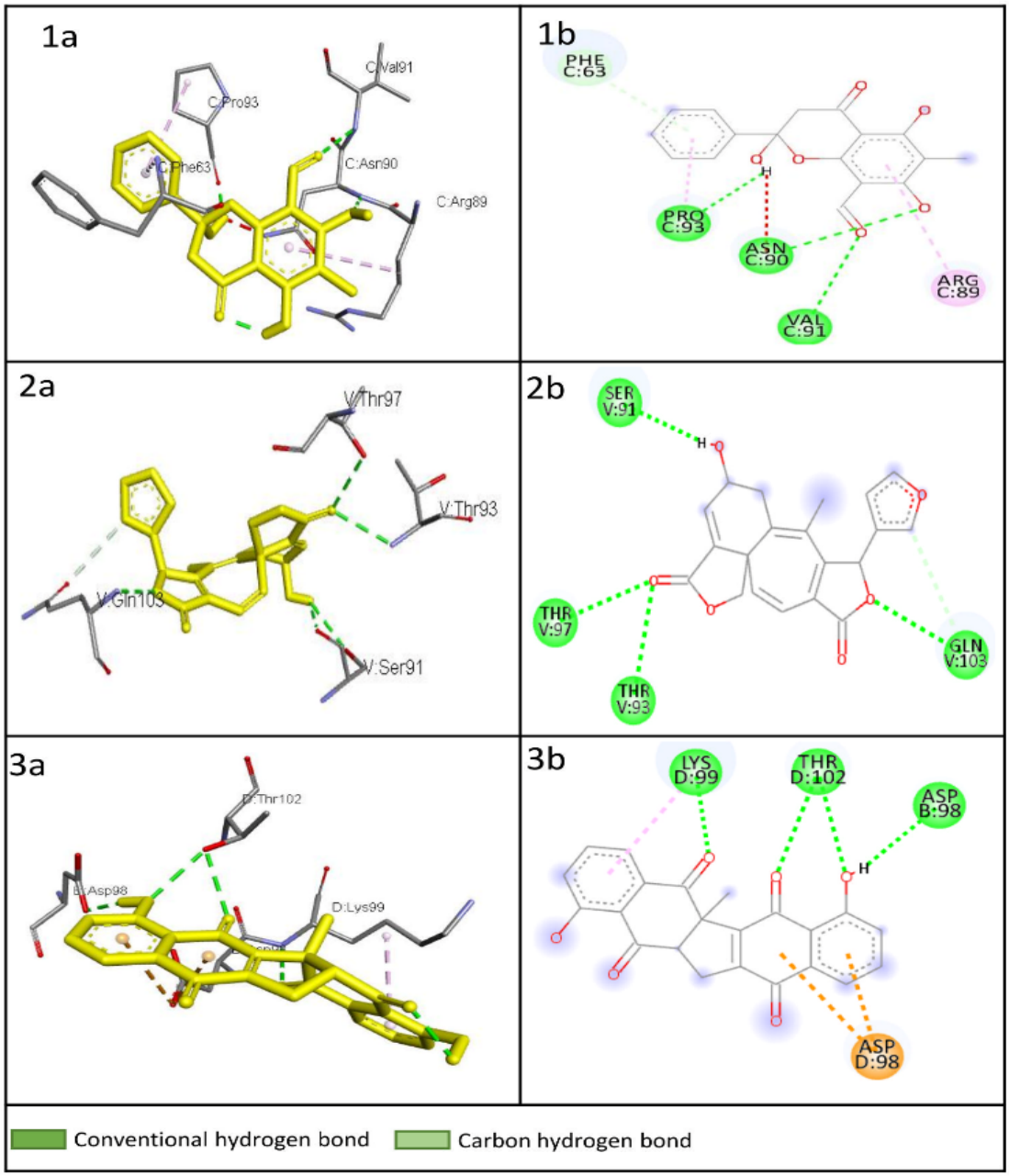

Figure 3. The interactions between the complexes those exhibited more hydrogen bonds with the proteins. a – 3D interactions; b – 2D interactions. 1 – Desmal with VP4, 2 – Salviandulin E with VP7, 3 – Zeylanone with NSP4.

3.5 Density Functional Theory Studies

In order to analyse the interactions evidenced in the docking results, a study on global and local chemical reactivity indices has been carried out.

The compound with higher chemical reactivity is the compound **Zeylanone** with a Hardness of -5,0025 eV and Hardness of 3,2469 eV, a Softness of 0,3079 eV^{-1} and electrophilicity of 3,8538 eV. These values are related to the docking results and the stabilization into the active site forming hydrogen (H) bonds. The compound with the lowest global chemical reactivity indices is the compound **Desmal** with a chemical reactivity of -4,1389 eV with Hardness of 4,4491 eV, Softness of 0,2247 eV^{-1} and electrophilicity of 1,9251 eV in **Table 4**. This compound also has a good stabilization on the active site like the compound **Zeylanone**. The other compound **Salviandulin E** in the docking model shows -H bonds formed. **Figure 4-6** are related to the Fukui Functions, Fukui function $f^-(r) \approx$

Square magnitude of the HOMO orbital, $|\varphi$ HOMO $(r)|^2$ means the susceptibility of the site to be attacked by electrophilic species, while the Fukui function f^+ (r) ≈ Square magnitude of the LUMO orbital, $|\varphi$ HOMO $(r)|^2$ represents the susceptibility of the site to be attacked by nucleophilic species.

For the compound **Zeylanone** the **Figure 6**, a) Fukui function f^- (r) ≈ Square magnitude of the HOMO orbital, $|\varphi$ HOMO $(r)|^2$ shows an isosurface on the right regions while the **Figure 6**, b), f^+ (r) ≈ Square magnitude of the LUMO orbital, $|\varphi$ HOMO $(r)|^2$ shows an isosurface on the left regions, showing two important regions for the stabilization process while the compounds **Desmal** and **Salviandulin E**, shows the same regions for the Fukui functions f^- (r) and f^+ (r) in **Figure 4.** (a) and 4(b) and **Figure 5.** (a) and 5 (b)). These contours understand the stabilization on the active site related to the -H bonds on the active site, and the electronic and steric effects by the substituent groups.

Table 4. Global Chemical Reactivity Indices

Compounds	PubChem ID	Chemical Potential (μ), eV	Hardness (η), eV	Softness (S), eV^{-1}	Electrophilicity (ω), eV
Desmal	10018499	-4,1389	4,4491	0,2247	1,9251
Salviandulin E	102251629	-4,4847	4,1568	0,2406	2,4192
Zeylanone	5276618	-5,0025	3,2469	0,3079	3,8538

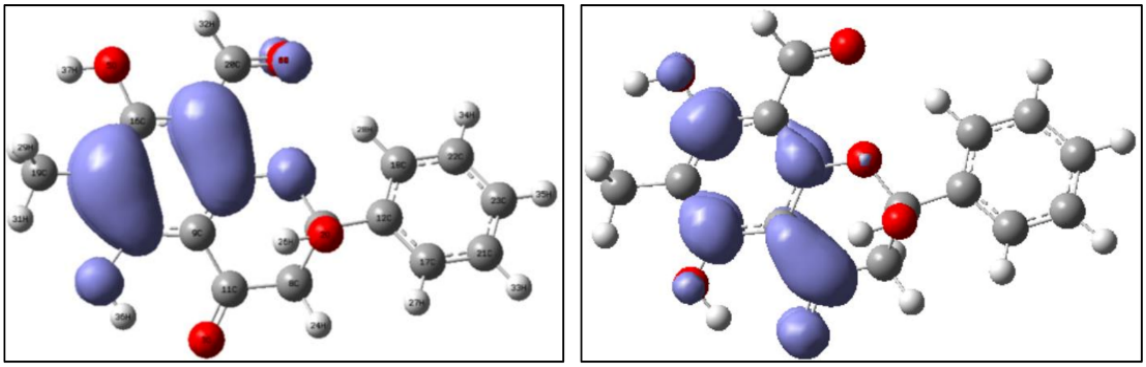

(a) ***fk-(r)≈HOMO2*** (b) ***fk+(r)≈LUMO2***

Figure 4. (a) *Fukui function* f^- (r) ≈ *Square* magnitude of the HOMO orbital, $|\varphi$ HOMO $(r)|^2$, is plotted on the 0.04. (b) *Fukui function* f^+ (r) ≈ *Square* magnitude of the LUMO orbital, $|\varphi$ HOMO $(r)|^2$, is plotted on the 0.04. For the compound Desmal.

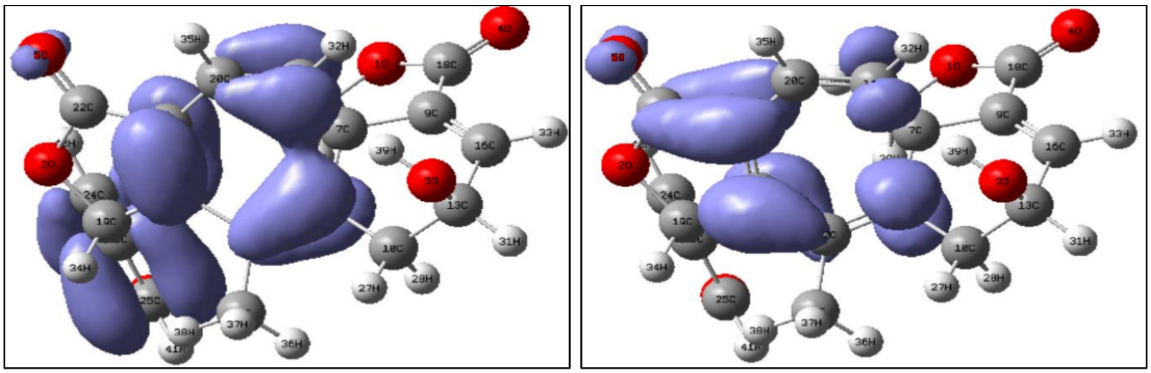

(a) ***fk-(r)≈HOMO2*** (b) ***fk+(r)≈LUMO2***

Figure 5. (a) *Fukui function* f^- (r) ≈ *Square* magnitude of the HOMO orbital, $|\varphi$ HOMO $(r)|^2$, is plotted on the 0.04. (b) *Fukui function* f^+ (r) ≈ *Square* magnitude of the LUMO orbital, $|\varphi$ HOMO $(r)|^2$, is plotted on the 0.04. For the compound Salviandulin E.

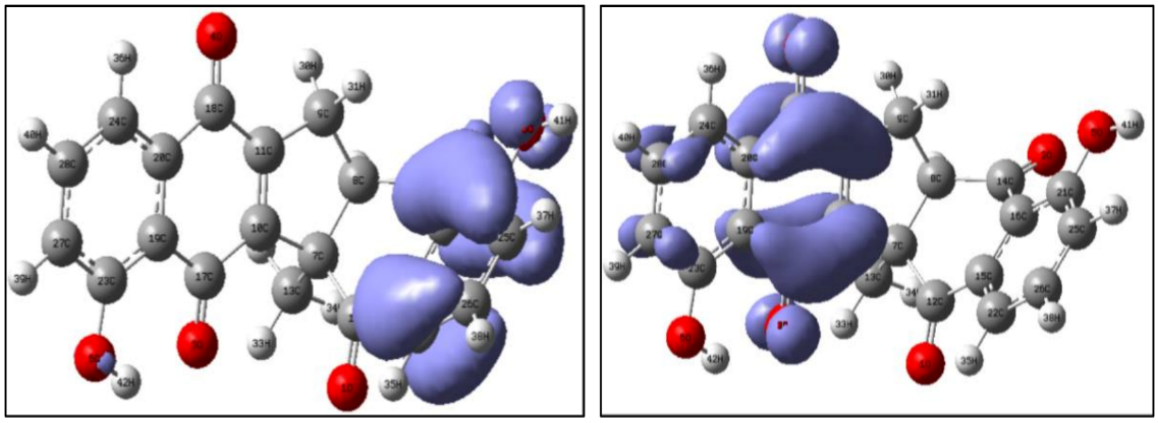

(a) *fk-(r)≈HOMO2* (b) *fk+(r)≈LUMO2*

Figure 6. (a) *Fukui function* f^- (r) ≈ *Square* magnitude of the HOMO orbital, |φ HOMO (r)|^2, is plotted on the 0.04. (b) *Fukui function* f^+ (r) ≈ *Square* magnitude of the LUMO orbital, |φ HOMO (r)|^2, is plotted on the 0.04. For the compound Zeylanone.

Conclusion

In this current research study, we applied the structure-based small molecule drug discovery methodology from plant PCs against the targets of the RV i.e., VP4, VP7 and NSP4. The tertiary structures of the viral proteins generated through homology modelling were used to find the binding affinity between the proteins and 396 PCs based on the drug-likeness rules such as Lipinski's rule, Ghose rule, GSK rule, Pfizer rule, Verber's rule, Egan's rule and QEDw. Based on the binding affinities and hydrogen bond interactions between the complex, three PCs have resulted as potent small molecules against viral proteins they are Desmal with VP4, Salviandulin E with VP7 and Zeylanone with NSP4. Among three compounds, Zeylanone exhibited two prior regions in stabilization compared to Desmal and Salviandulin E. However, in the present study based on the Insilico studies, the PCs Desmal, Salviandulin E and Zeylanone can be further exploited in advancement as a potent drug against the hetero-oligomer complex.

Funding: This research received no external funding.

Disclosure statement: *Conflicts of Interest:* The authors declare no conflict of interest.
Compliance with Ethical Standards: This article does not conrain any studies involving human or animal subjects.

References

Aoyagi Y., Fujiwara K., Yamazaki A. (2014) Semisynthesis of salviandulin E analogues and their antitrypanosomal activity. *Bioorg Med Chem Lett,* 24(2), 442-446.

Bickerton G. R., Paolini G. V., Besnard J., Muresan S., Hopkins A. L. (2012) Quantifying the chemical beauty of drugs. *Nat Chem,* 4(2), 90-98. doi:10.1038/nchem.1243.

Bienert S., Waterhouse A., de Beer T.A., Tauriello G., Studer G., Bordoli L., Schwede T. (2017) The SWISS-MODEL Repository - new features and functionality, *Nucleic Acids Res,* 45(1): 313-319. https://doi.org/10.1093/nar/gkw1132.

Cetina-Montejo L *et al.,* Zeylanone epoxide isolated from Diospyros anisandra stem bark inhibits influenza virus in vitro, *Arch Virol* 164(6):1543-1552, 2019. https://doi.org/10.1007/s00705-019-04223-y.

Chattaraj P. K., Sarkar U., Roy D. R. (2006) Electrophilicity index, *Chem. Rev,* 106:2065-209. https://doi.org/10.1021/cr040109f.

Chattaraj, P. K., Maiti B., Sarkar U. (2013) Philicity: A Unified Treatment of Chemical Reactivity and Selectivity. *J. Phys. Chem. A* 107, 4973, 1089-5639. doi: 10.1021/jp034707u.

Cook S. M., Glass R. I., LeBaron C. W., Ho M. S. (1990) Global seasonality of rotavirus infections, Bulletin of the World Health Organization, *68*(2): 171–177. doi:10.1021/jm020017n.

Diass K., Oualdi I., Dalli M., Azizi S.-Ed, Mohamed M., Gseyra N., Touzani R., Hammouti B. (2023) Artemisia herba alba Essential Oil: GC/MS analysis, antioxidant activities with molecular docking on S protein of SARS-CoV-2, *Indonesian Journal of Science & Technology* 8(1), 1-18

Egan W. J., Merz K. M., Jr Baldwin J. J. (2000) Prediction of drug absorption using multivariate statistics. *J Med Chem,* 43(21):3867-3877. doi:10.1021/jm000292e.

Estes M. K., Greenberg H. B. , Rotaviruses. In Fields Virology, 6th ed.; edited by Knipe, D.M.; Howley, P.M. Wolters Kluwer Health /Lippincott Williams & Wilkins, *Philadelphia* 2003, pp. 1347-1401. https://doi.org/10.1053/j.gastro.2009.02.076.

Frisch M. J., Trucks G. W., Schlegel H. B., Scuseria G. E., Robb M. A., Cheeseman J. R., Scalmani G., Barone V., Mennucci B., Petersson G. A., Nakatsuji H., Caricato M., Li X., Hratchian H. P., Izmaylov A. F., Bloino J., Zheng G., Sonnenberg J. L., Hada M., Ehara M., Toyota K., Fukuda R., Hasegawa J., Ishida M., Nakajima T., Honda Y., Kitao O., Nakai H., Vreven T., Montgomery Jr., J .A., Peralta J. E., Ogliaro F., Bearpark M., Heyd J. J., Brothers E., Kudin K. N., Staroverov V. N., Kobayashi R., Normand J., Raghavachari K., Rendell A., Burant J. C., Iyengar S. S., Tomasi J., Cossi M., Rega N., Millam J. M., Klene M., Knox J. E., Cross J. B., Bakken V., Adamo C., Jaramillo J., Gomperts R., Stratmann R. E., Yazyev O., Austin A. J., Cammi R., Pomelli C., Ochterski J. W., Martin R. L., Morokuma K., Zakrzewski V. G., Voth G. A., Salvador P., Dannenberg J. J., Dapprich S., Daniels A.D., Farkas O., Foresman J. B., Ortiz J. V., Cioslowski J. Fox D. J. (2010) Gaussian 09, Revision B.01. Gaussian Inc., Wallingford.Aoyagi Y., Fujiwara K., Yamazaki A. (2014) Semisynthesis of salviandulin E analogues and their antitrypanosomal activity. *Bioorg Med Chem Lett,* 24(2):442-446. https://doi.org/10.1016/j.bmcl.2013.12.052.

Fuentealba P., Pérez P., Contreras R. (2022) Critical thoughts on computing atom condensed Fukui functions, *J. Chem. Phys* 113: 2544. https://doi.org/10.1063/1.2749518.

Galván M., Pérez P., Contreras R., Fuentealba P. (2000) A direct evaluation of regional Fukui functions in molecules. *Chem. Phys. Lett,* 30:405-413.

Geerlings P., De Proft F., Langenaeker W. (2013) Conceptual density functional theory. *Chem. Rev,* 103:1793–1873. https://doi.org/10.1021/cr990029p.

Ghose A. K., Viswanadhan V. N., Wendoloski J. J. (1999) A knowledge-based approach in designing combinatorial or medicinal chemistry libraries for drug discovery. 1. A qualitative and quantitative characterization of known drug databases, *Journal of Combinatorial Chemistry,* 1 (1), 55–68. doi:10.1021/cc9800071.

Graham K. L., Halasz P., Tan Y., Hewish M.J., Takada Y., Mackow E.R., Robinson M. K., Coulson B.S. (2003) Integrin-using rotaviruses bind a2b1 integrin a2 I domain via VP4 DGE sequence and recognize aXb2 and aVb3 by using VP7 during cell entry. J Virol. 77:9969–9978. https://doi.org/10.1128/jvi.77.18.

Isanaka S., Guindo O., Langendorf C., Matar Seck A., Plikaytis B.D., Sayinzoga-Makombe N., McNeal M. M., Meyer N., Adehossi E., Djibo A. (2017) Efficacy of a low-cost, heat-stable oral rotavirus vaccine in Niger, *N. Engl. J. Med,* 376, 1121–1130. https://doi.org/10.1056/NEJMoa1609462.

Kirkwood CD. (2010) Genetic and antigenic diversity of human rotaviruses: potential impact on vaccination programs, The Journal of infectious diseases, 202, 43–48, 2010. https://doi.org/10.1086/653548.

Li Y. J., Ma G. P., Li G. W., Qiao X. Y., Ge J. W., Tang L.J., Liu M., Liu L. W. (2010) Oral vaccination with the porcine rotavirus VP4 outer capsid protein expressed by Lactococcus lactis induces specific antibody production, J. Biomed. Biotechnol, 708460, 2010. https://doi.org/10.1155/2010/708460.

Lipinski C. A. (2004) Lead- and drug-like compounds: the rule-of-five revolution, *Drug Discovery Today: Technologies* 1(4), 337–341. doi:10.1016/j.ddtec.2004.11.007.

Maass D. R., Atkinson P. H. (1990) Rotavirus proteins VP7, NS28, and VP4 form oligomeric structures, J. Virol 64, 2632-2641. https://doi.org/10.1128/JVI.64.6.2632-2641.1990.

Matthijnssens J., Ciarlet M., Heiman E., Arijs I., Delbeke T., McDonald S. M., Palombo E. A., Iturriza-Gómara M., Maes P., Patton J. T., Rahman M., Van Ranst M. (2008) Full genome-based classification of rotaviruses reveals a common origin between human Wa-Like and porcine rotavirus strains and human DS-1-like and bovine rotavirus strains. J. Virol. 82:3204-3219. https://doi.org/10.1128/JVI.02257-07.

Medeiros R. S., França Y., Viana E. (2023) Genomic Constellation of Human Rotavirus G8 Strains in Brazil over a 13-Year Period: Detection of the Novel Bovine-like G8P[8] Strains with the DS-1-like Backbone, *Viruses* 15(3): 664. https://doi.org/10.3390/v15030664.

Merzouki M., Challioui A., Bourassi L., Abidi R., Bouammli B., El Farh L. (2023) In silicoevaluation of antiviral activity of flavone derivatives and commercial drugs against SARS-CoV-2 main protease (3CLpro), *Mor. J. Chem.,* 14(1), 129-143. https://doi.org/10.48317/IMIST.PRSM/morjchem-v11i1.35278

Morales-Bayuelo A., Baldiris R., Vivas-Reyes R. (2013) Scale Alpha and Beta of Quantitative Convergence and Chemical Reactivity Analysis in Dual Cholinesterase/Monoamine Oxidae Inhibitors for the Alzheimer Disease Treatment Using Density Functional Theory (DFT). *J. Theor. Chem,* 3:1-13. doi:10.1155/2013/768185.

Morales-Bayuelo A., Torres J., Baldiris R., Vivas-Reyes R. (2017) New insights to understand the CoMFA and CoMSIA análisis within the framework of Density Functional Theory. Toward a generalized methodology. *Int. J. Quant. Chem,* 112: 2681. http://dx.doi.org/10.3390/mol2net-03-03905.

Morales-Bayuelo A., Torres J., Vivas-Reyes R. (2012) Hückel treatment of pyrrole and pentalene as a function of cyclopentadienyl using local quantum similarity index (LQSI) and the topo-geometrical superposition approach (TGSA). *J. Theo. Comp. Chem,* 11:223. https://doi.org/10.1142/S0219633612500150.

Morales-Bayuelo A., Torres j., Vivas-Reyes R. (2012) Quantum molecular similarity analysis and quantitative definition of catecholamines with respect to biogenic monoamines associated: Scale alpha and beta of quantitative convergence. *Int. J. Quant. Chem,* 112:2637- 42. https://doi.org/10.1002/qua.23284.

Morales-Bayuelo A., Vivas-Reyes R. (2013) Theoretical model for the polarization molecular and Hückel treatment of PhosphoCyclopentadiene in an external electric field: Hirschfeld study. *J. Math. Chem,* 51:1835-1852. https://doi.org/10.1007/s10910-013-0182-3.

Morales-Bayuelo A., Vivas-Reyes R. (2014) Mathematical Analysis of a Series of 4-Acetylamino-2-(3,5-dimethylpyrazol-1-yl)-6-pyridylpyrimidines: A Simple WAY TO Relate Quantum Similarity to Local Chemical Reactivity Using the Gaussioan Orbitals Localized Theory. *J. Quant. Chem,* Article ID 850163, 12 pages. https://doi.org/10.1155/2014/624891.

Morales-Bayuelo A., Vivas-Reyes R. (2014) Theoretical Calculations and Modelling for the Molecular Polarization of Furan and Thiophene under the Acction of an Electric Field Using Quantum Similarity. *J. Quant. Chem,* 1-3, Article ID 585394. doi:10.1155/2014/585394.

Morales-Bayuelo A., Vivas-Reyes R. (2014) Understanding the Polar Character Trend in a Series of Diels-Alder Reactions Using Molecular Quantum Similarity and Chemical Reactivity Descriptors. *J. Quant. Chem,* Article ID 239845, 19 pages. https://doi.org/10.1155/2014/239845.

Najmi A., Javed S.A., Al Bratty M., Alhazmi H.A. (2022) Modern Approaches in the Discovery and Development of Plant-Based Natural Products and Their Analogues as Potential Therapeutic Agents, *Molecules* 27(2), 349, 2022. https://doi.org/10.3390/molecules27020349.

O'Ryan M., Linhares A. C. (2009) Update on Rotarix: an oral human rotavirus vaccine. Expert Rev, *Vaccines* 8, 1627–1641. https://doi.org/10.1586/erv.09.136.

O'Boyle N. M., Banck M., James C. A., Morley C., Vandermeersch T., Hutchison G. R. (2011) Open Babel: An open chemical toolbox, *J Cheminform* 3, 33, 2011. doi:10.1186/1758-2946-3-33.

Parashar U. D., Gibson C. J., Bresee J. S., Glass R. I. (2006) Rotavirus and severe childhood diarrhoea. Emerging infectious diseases, 12(2):304–306.

Parr R. G., Pearson R. G. (1983) Absolute hardness: companion parameter to absolute electronegativity. *J. Am. Chem Soc,* 105: 7512-7516. https://doi.org/10.1021/ja00364a005.

Parr R. G., Szentpaly L. V., Liu S. (1999) Electrophilicity Index. *J. Am. Chem. Soc,* 121: 1922-1924. https://doi.org/10.1021/ja983494x.

Pettersen E. F., Goddard T. D., Huang C. C., Couch G. S., Greenblatt D. M., Meng E.C., Ferrin T. E. (2004) UCSF Chimera--a visualization system for exploratory research and analysis. *J Comput Chem,* 25(13): 1605-12. https://doi.org/10.1002/jcc.20084.

Poruchynsky M. S., Maass D. R., Atkinson P. H. (1991) Calcium depletion blocks the maturation of rotavirus by altering the oligomerization of virus-encoded proteins in the ER. J. Cell Biol, 114, 651-656. https://doi.org/10.1083/jcb.114.4.651.

Radoslav K., David H. (2018) P2Rank: machine learning based tool for rapid and accurate prediction of ligand binding sites from protein structure. *J. Cheminformatics,* 10(1):39. https://doi.org/10.1186/s13321-018-0285-8.

Troeger C., Khalil I. A., Rao P. C., Cao S., Blacker B. F., Ahmed T., Armah G., Bines J. E., Brewer T. G., Colombara D. V., Kang G., Kirkpatrick B. D., Kirkwood C. D., Mwenda J. M., Parashar U. D., Petri W. A., Jr Riddle M. S., Steele A. D., Thompson R. L., Walson J. L., Reiner R. C. (2018) Rotavirus Vaccination and the Global Burden of Rotavirus Diarrhoea Among Children Younger Than 5 Years, JAMA pediatrics, *172*(10): 958–965. https://doi.org/10.1001/jamapediatrics.2018.1960.

Trott O., Olson A. J. (2010) Autodock Vina: improving the speed and accuracy of docking with a new scoring function, efficient optimization, and multithreading. *J Comput Chem,* 31(2):455-461. https://doi.org/10.1002/jcc.21334.

Veber D. F., Johnson S. R., Cheng H. Y., Smith B. R., Ward K. W., Kopple K. D. (2002) Molecular properties that influence the oral bioavailability of drug candidates. *Journal of Medicinal Chemistry,* 45 (12):2615–2623.

Vélez LA *et al.,* (2022) Theoretical Prediction of Gastrointestinal Absorption of Phytochemicals. *Int. J. Plant Biol 13*:163-179. https://doi.org/10.3390/ijpb13020016.

Vetter J., Papa G., Seyffert M., Gunasekera K., De Lorenzo G., Wiesendanger M., Reymond J. L., Fraefel C., Burrone O. R., Eichwald C. (2022) Rotavirus Spike Protein VP4 Mediates Viroplasm Assembly by Association to Actin Filaments. Journal of virology *96*(17). https://doi.org/10.1128/jvi.01074-22.

Vlasova A. N., Amimo J. O., Saif L.J. (2010) Porcine rotaviruses: epidemiology, immune responses and control strategies, Viruses 48 (9).

Yukawa T., Naven R. (2020) Utility of Physicochemical Properties for the Prediction of Toxicological Outcomes: Takeda Perspective, *ACS Med Chem Lett,* 11(2):203-209. doi:10.1021/acsmedchemlett.9b00536.

Zhang X., Settembre E., Xu C., Dormitzer P.R., Bellamy R., Harrison S. C., Grigorieff N. (2018) Near-atomic resolution using electron cryomicroscopy and singleparticle reconstruction, Proc Natl Acad Sci, 105, 1867–1872. https://doi.org/10.1073/pnas.0711623105.